fibroelastosis of RV muscles [6]. However, how RV stiffness influences the postoperative hemodynamics has not been reported. Given the small number of patients with each of the wide variety of preoperative RV conditions [7, 8], the influence of RV stiffness on 1.5VR, 2VR, and Fontan operation cannot be examined by clinical study. It is also difficult to experimentally reproduce hemodynamics before and after 1.5VR for hypoplastic RV with various stiffness. In view of the above, we attempted to clarify postoperative hemodynamics by a theoretical analysis using a computational model based on lumped-parameter state-variable equations. The present results indicate that the RV stiffness constant may provide selection criteria for 1.5VR.

Materials and methods

The electrical analogs of the model used to simulate the cardiovascular system are shown in Fig. 1. We modeled the postoperative cardiovascular system mathematically by a combination of the time-varying elastance cardiac chamber model and the three-element Windkessel vascular model. We set the normal values of parameters to be appropriate for a 75-kg man. These values were obtained from the literature [9–13] and are listed in Table 1. Since the data of the pressure–volume relationship of the atrium were scarcely available, parameters of the atrium were surmised from the literature [10–12].

Heart

The right and left ventricular chambers as well as the atrial chambers are represented by the time-varying elastance model [9, 10, 13]. The end-systolic pressure–volume relationship is described by a linear formula:

$$P_{es,cc} = E_{es,cc}\left[V_{es,cc} - V_{0,cc}\right] \quad (1)$$

where $P_{es,cc}$ and $V_{es,cc}$ are end-systolic pressure and volume, respectively; $E_{es,cc}$ is the maximal volume elastance; $V_{0,cc}$ is the volume at which $P_{es,cc}$ is equal to 0 mmHg. cc denotes each chamber, i.e., RA for the right atrium, LA for the left atrium, RV for the right ventricle, or LV for the left ventricle. The end-diastolic pressure–volume relationship is represented by a non-linear formula:

$$P_{ed,cc} = A_{cc}\left[e^{B_{cc}(V_{ed,cc}-V_{0,cc})} - 1\right] \quad (2)$$

where $P_{ed,cc}$ and $V_{ed,cc}$ are end-diastolic pressure and volume, respectively; A_{cc} and B_{cc} are constants [9, 10, 13]. We assumed the time course of the time-varying elastance by defining normalized elastance curve $e_{cc}(t)$ as:

Table 1 Parameters used in modeling

Heart rate (HR), beats/min	75			
Duration of cardiac cycle (T_c), ms	800			
Time advance of atrial systole (DT), ms	16			
Total stressed blood volume (V_s), ml	750	(control only)		
	LV	RV	LA	RA
Time to end systole (T_{es}), ms	200	200	120	120
End-systolic elastance (E_{es}), mmHg/ml	3.0	0.7	0.5	0.5
Scaling factor of EDPVR (A), mmHg	0.35	0.35	0.06	0.06
Exponent scaling factor for EDPVR (B), ml^{-1}	0.033	0.023	0.264	0.264
Unstressed volume (V_0), ml	0	0	5	5
	Aortic	Pulmonary	Mitral	Tricuspid
Valvular resistance (forward), (mmHg s)/ml	0.001	0.001	0.001	0.001
	Systemic		Pulmonary (p)	
	Superior (ss)	Inferior (si)		
Arterial resistance (R_a), (mmHg s)/ml	2.25	1.5	0.03	
Characteristic impedance (R_c), (mmHg s)/ml	0.075	0.05	0.02	
Venous resistance (R_v), (mmHg s)/ml	0.0375	0.025	0.015	
Arterial capacitance (C_a), ml/mmHg	0.528	0.792	13	
Venous capacitance (C_v), ml/mmHg	28	42	8	

LV Left ventricle, *RV* right ventricle, *LA* left atrium, *RA* right atrium, *EDPVR* end-diastolic pressure–volume relationship

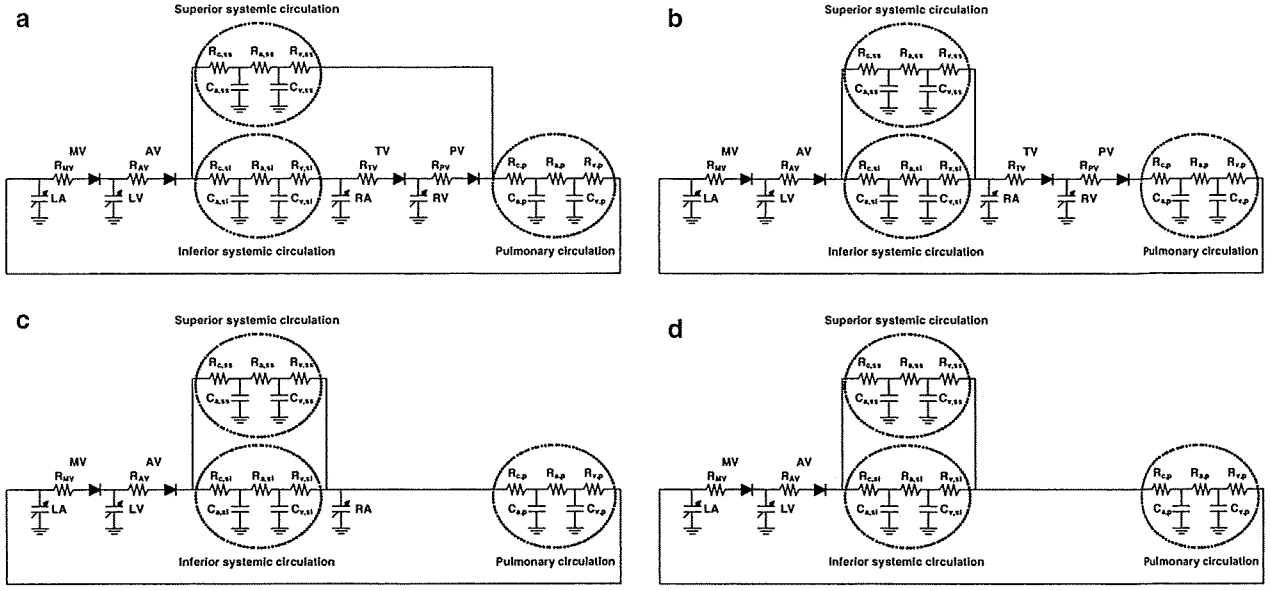

Fig. 1 **a** The electric equivalent circuit of one and a half ventricle repair. **b** Biventricular repair (normal circulation). **c,d** Variations of Fontan operation [**c** atriopulmonary connection (APC); **d** total cavopulmonary connection (TCPC)]. *LV* and *RV* left and right ventricles, *LA* and *RA* left and right atria, *AV* and *MV* aortic and mitral valves, *PV* and *TV* pulmonary and tricuspid valves, C_a and C_v lumped arterial and venous capacitances, R_c characteristic impedances, R_a lumped arterial resistances, R_v venous resistances, *ss* superior systemic circulation, *si* inferior systemic circulation, *p* pulmonary circulation

$$e_{cc}(t) = 0.5[1 - \cos(\pi t/T_{es,cc})]\ (0 \le t < 2T_{es,cc})$$
$$e_{cc}(t) = 0\ (2T_{es,cc} \le t < T_c) \quad (3)$$

where t is the time from the start of systole, $T_{es,cc}$ is the duration of systole, and T_c is the duration of cardiac cycle. Using $e_{cc}(t)$, the instantaneous pressure, $P_{cc}(t)$, is described by:

$$P_{cc}(t) = [P_{es,cc}(V_{cc}) - P_{ed,cc}(V_{cc})]e_{cc}(t) + P_{ed,cc}(V_{cc}) \quad (4)$$

Ventricular systole is preceded by atrial systole. The time advance of atrial systole (DT) is calculated as the fixed fraction of T_c (DT = $0.02T_c$). Function of each chamber is characterized by the parameters $E_{es,cc}$, $T_{es,cc}$, $V_{0,cc}$, A_{cc}, B_{cc}, and $e_{cc}(t)$. The same $e_{cc}(t)$ was used for all chambers, but the other parameters were different between chambers, as shown in Table 1.

Vascular system

Basically, the pulmonary and systemic circulations are modeled as modified Windkessel impedances. Each vascular system is modeled by lumped venous (C_v) and arterial (C_a) capacitances, a characteristic impedance (R_c) that is related to the stiffness of the proximal aorta or pulmonary artery, a lumped arterial resistance (R_a), and a resistance proximal to C_v (R_v). This framework is similar to that used in deriving Guyton's resistance to venous return [14].

To simulate the postoperative hemodynamics of 1.5VR, the systemic circulation is divided into two parts, the superior and the inferior circulation. Therefore, the parameters of the systemic circulation are also divided into the superior and inferior ones, as shown in Fig. 1. Blood flow in the descending aorta is reported to be 63.8% of the left ventricular output [15]. The compliance of the IVC is considered to be 66.6% of the total venous compliance [16]. Thus, in our model, arterial and venous compliances of the inferior systemic circulation are adjusted to 0.6 times those of the compliance of the total circulation, and the blood flow of the inferior systemic circulation is controlled to be 60% of the left ventricular output by adjusting the resistances of R_c, R_a, and R_v.

The capacitance of the superior systemic circulation is also divided into arterial ($C_{a,ss}$) and venous ($C_{v,ss}$). Similarly, arterial and venous capacitances are defined for the inferior systemic circulation ($C_{a,si}$ and $C_{v,si}$) and for the pulmonary circulation ($C_{a,p}$ and $C_{v,p}$). The ratio of C_a to C_v was obtained from the literature [9, 10, 13]. The relationship between pressure (P_c) and volume (V_c) in each capacitance is described by the following linear formula.

$$P_c = \frac{V_c}{C} \quad (5)$$

The changes in volume in each capacitance ($dV(t)/dt$) are described by the differential equations below

$$\frac{dV(t)}{dt} = \sum Q_{\text{in-flow}}(t) - \sum Q_{\text{out-flow}}(t) \quad (6)$$

where $\Sigma Q_{\text{in-flow}}(t)$ and $\Sigma Q_{\text{out-flow}}(t)$ indicate the sum of instantaneous volumetric flow rates at the inlet and outlet of each compartment, respectively. Each of the aortic, mitral, pulmonary, and tricuspid valves is described as an ideal diode with a serially connected small resistor.

In the 1.5VR model, the superior circulation flows from SVC to PA, while the inferior blood flow returns to RA through IVC as shown in Fig. 1a. The models of 2VR (Fig. 1b) and variations of Fontan operation [Fig. 1c, atriopulmonary connection (APC); Fig. 1d, total cavopulmonary connection (TCPC)] are constructed for comparisons. Although the superior and inferior systemic circulations return to RA in both 2VR and APC models, RA is directly connected to PA in the APC model. In the TCPC model, SVC and IVC are directly connected to PA. All parameter values were the same for all of these models except total stressed blood volume (see below) (Table 1).

Hypoplastic RV

Hypoplastic RV is physiologically characterized by an increase in RV stiffness caused by hypertrophy and fibroelastosis of RV muscles [6]. Recalling Eq. 2 for RV, we have:

$$P_{\text{ed,RV}} = A_{\text{RV}}\left[e^{B_{\text{RV}}\left(V_{\text{ed,RV}} - V_{0,\text{RV}}\right)} - 1\right] \quad (7)$$

where B_{RV} is stiffness constant of RV. The value of B_{RV} was changed stepwise from 0.023/ml (normal RV) to 0.143/ml (extremely stiff RV) in increments of 0.01/ml to simulate the various degrees of RV stiffness associated with hypoplasia (Fig. 2).

Protocols

First, the control state was simulated by the 2VR model with normal RV stiffness constant ($B_{\text{RV}} = 0.023$). The total stressed blood volume (V_s), equal to the sum of the stressed volumes in each capacitance and the volume of each chamber, was set as 750 ml to reproduce normal hemodynamics.

$$V_s = V_{\text{LV}} + V_{\text{RV}} + V_{\text{LA}} + V_{\text{RA}} + V_{\text{Ca,ss}} + V_{\text{Cv,ss}} + V_{\text{Ca,si}} + V_{\text{Cv,si}} + V_{\text{Ca,p}} + V_{\text{Cv,p}} \quad (8)$$

We solved these simultaneous equations (Eqs. 1–8) using the component ODE45 of MATLAB, based on the Runge–Kutta method (MathWorks). The hemodynamic parameters of 2VR with normal RV stiffness constant are listed in Table 2.

Next, systemic cardiac output, pulmonary arterial pressure (PAP), right atrial pressure (RAP), and RVEDV after each procedure were calculated for each RV stiffness constant. Heart rate was kept constant and mean systemic arterial pressure (MAP) was controlled at the same value as that of the control state, by adjusting the total stressed blood volume.

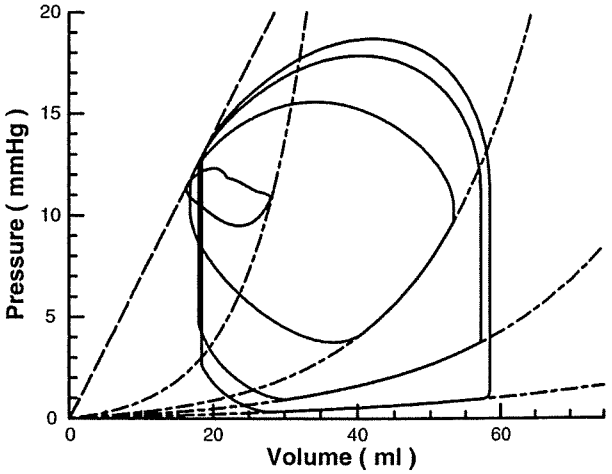

Fig. 2 Right ventricular pressure–volume loops (PV loop) after one and a half ventricle repair. With the increase in the right ventricular stiffness constant, the PV loop became smaller. The *horizontal axis* is the instantaneous right ventricular volume (ml) and the *longitudinal axis* is the instantaneous right ventricular pressure (mmHg)

Table 2 Control hemodynamic parameters (2VR with normal RV stiffness constant)

Parameter	Value
Heart rate (HR), beats/min	75
Mean systemic arterial pressure (MAP), mmHg	80.3
Mean pulmonary arterial pressure (PAP), mmHg	13.6
Mean right atrial pressure (RAP), mmHg	2.34
Mean left atrial pressure (LAP), mmHg	8.26
Left ventricular cardiac output (CO), l/min	4.95

Results

Figure 3a shows the impact of the RV stiffness constant on systemic cardiac output after each procedure. In the Fontan circulation (APC and TCPC), systemic cardiac output was independent of the RV stiffness constant and remained at 4.40 l/min. Under the condition of normal RV stiffness constant, systemic cardiac output was 4.95 l/min in 2VR and 4.73 l/min in 1.5VR, being 13 and 8% greater than that of Fontan circulation, respectively. As the RV stiffness constant was increased from the control value to mimic increased severity of RV

hypoplasia, systemic cardiac output decreased in both 2VR and 1.5VR circulations. Within the range between 100 and 150% of the control RV stiffness constant, systemic cardiac output of 2VR circulation was obviously greater than those of other two circulations. With the RV stiffness constant >150%, systemic cardiac output became greater in 1.5VR than in 2VR. In this situation, 2VR needed larger stressed blood volume than 1.5VR to maintain MAP (Fig. 3d).

The results for PAP and RAP are shown in Fig. 3b. As the RV stiffness constant increased, PAP decreased and RAP increased in both 2VR and 1.5VR circulations. In 2VR circulation, RAP increased steeply as the RV stiffness constant increased up to 150% of normal, and exceeded the atrial pressure of TCPC when the RV stiffness constant increased above 150% of normal. In 1.5VR circulation, RAP also increased but more slowly and exceeded the atrial pressure of TCPC only when the RV stiffness constant increased above 250% of normal. PAP in 1.5VR circulation, which was equal to SVC pressure, became higher than PAP in 2VR circulation in the range of RV stiffness constant >150% of normal.

In the control state, RVEDV in 2VR was 87.7 ml, which was treated as the value of 100% of RVEDV. The influence of the RV stiffness constant on RVEDV is shown in Fig. 3c. In 2VR circulation, RVEDV decreased as the RV stiffness constant increased. In 1.5VR circulation, RVEDV reduced only slightly with an increase in the RV stiffness constant until 250% of normal. In the range of RV stiffness constant >250% of normal, RVEDV showed a relatively linear decay in both 2VR and 1.5VR circulations, and there was no difference in RVEDV between 2VR and 1.5VR. In this situation, both 1.5VR and 2VR needed larger stressed blood volume than Fontan circulation (Fig. 3d).

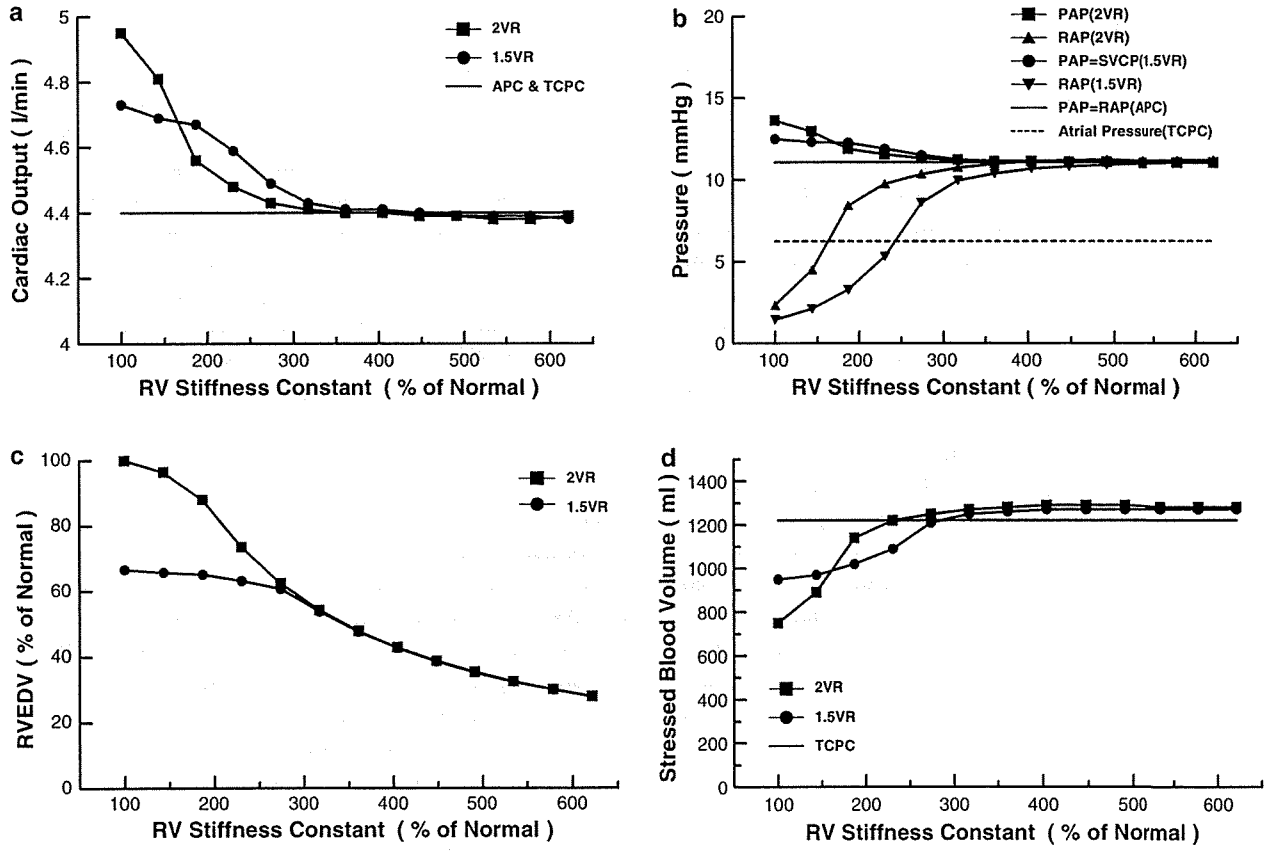

Fig. 3 **a** The relationship between systemic cardiac output (l/min) and % stiffness constant of hypoplastic right ventricle. The *horizontal axis* is the ratio of RV stiffness constant (% stiffness constant) to the normal value. **b** The relationship between pulmonary arterial pressure or right atrial pressure (mmHg) and % stiffness constant of hypoplastic RV. Pulmonary arterial pressure is the same as right atrial pressure in APC. **c** The relationship between % RVEDV and % stiffness constant of hypoplastic RV. **d** The relationship between stressed blood volume (ml) and % stiffness constant. *2VR* biventricular repair, *1.5VR* one and a half ventricle repair, *APC* and *TCPC* variations of Fontan operation (*APC* atriopulmonary connection, *TCPC* total cavopulmonary connection); *PAP* pulmonary arterial pressure, *RAP* right atrial pressure, *SVCP* superior vena caval pressure, *RVEDV* right ventricular end-diastolic volume

Discussion

The results of this theoretical analysis suggest that, in patients with hypoplastic RV, postoperative hemodynamics depends largely on the RV stiffness constant. PA/IVS, Ebstein's anomaly or their relatives are characterized by varying degrees of underdevelopment of RV. For a severely hypoplastic RV, the definitive treatment is single ventricular circulation. For a mildly hypoplastic RV, biventricular circulation is expected to have merit. Recently, 1.5VR has been proposed to reduce the surgical risk of 2VR. The use of 1.5VR has lowered the early or midterm mortality, and adequate growth of RV and the tricuspid valve has been documented in some patients [2]. However, the postoperative RV dysfunction or arrhythmic event has also been reported, in particular, when the patients are on the borderline of criteria between 1.5VR and Fontan operation [4, 5].

For the choice of surgical options among Fontan operation, 1.5VR, and 2VR, the previously used criteria were based on morphologic characteristics of the hypoplastic RV, such as RVEDV. However, simple anatomic indices may be inaccurate, since these values are dependent on the afterload and preload conditions. For that reason, the treatment strategy for hypoplastic RV based on the anatomic indices remains controversial. We focused on the intrinsic property of hypoplastic RV, i.e., RV stiffness constant. The fact that the RV stiffness constant, an index of chamber property, is relatively independent of the loading condition is important for the accurate prediction of postoperative hemodynamics. Based on the results of the present study, we propose that patients with hypoplastic RV can be classified into three groups according to the RV stiffness constant. The first group consists of patients with mild RV hypoplasia (RV stiffness constant <150% of normal), in whom enlargement of RV is expected after the operation. At the other extreme, the second group consists of patients with severe RV hypoplasia (RV stiffness constant >250%), in whom no RV reconstruction is expected to have merit. In addition, we have shown that there certainly exists a third group consisting of patients with intermediate RV hypoplasia (RV stiffness constant between 150 and 250%), who would benefit more from 1.5VR than from 2VR or Fontan operation.

Mild RV hypoplasia

When RV hypoplasia is mild (RV stiffness constant <150% of normal), systemic cardiac output is greater in 2VR than in 1.5VR or Fontan operation (APC or TAPC). Therefore, we recommend that 2VR should be chosen in the mild RV hypoplasia group. Although systemic cardiac output in 1.5VR is also greater than that in Fontan operation, SVC pressure (which is equal to PAP) is higher than that of APC. Accordingly, the upper part of the body is exposed to higher SVC pressure in 1.5VR, which may cause postoperative pleural effusion [2]. A large pressure gradient between SVC and IVC also results in abnormal venous collaterals from SVC to IVC [17–20], and they could effectively increase the venous return to RA in 1.5VR.

Intermediate RV hypoplasia

When RV hypoplasia is intermediate (RV stiffness constant between 150 and 250% of normal), systemic cardiac output in 1.5VR exceeds that in 2VR. Although SVC pressure is still higher in 1.5VR than in APC, RAP is lower in 1.5VR than in the other procedures. This condition is favorable to reduce supraventricular arrhythmias related to high RAP during the perioperative periods. This beneficial effect is not expected for 2VR since RAP in 2VR is higher than the atrial pressure of TCPC. Furthermore, 1.5VR is advantageous from the viewpoint of stressed blood volume because 1.5VR needs smaller stressed blood volume than does 2VR to maintain MAP (Fig. 3d).

In these patients, RVEDV in 1.5VR is relatively independent of the RV stiffness constant. However, abnormal systemic venous collateral channels might open after 1.5VR. These collateral channels would increase RV preload wastefully and decrease systemic cardiac output in the late postoperative phase. In such conditions, conversion to the Fontan circulation may be required in the late phase [4, 5]. Nevertheless, 1.5VR should be recommended for the intermediate RV hypoplasia group because high cardiac output and low RAP are anticipated.

Severe RV hypoplasia

When RV hypoplasia is severe (RV stiffness constant >250% of normal), neither 1.5VR and 2VR are expected to improve systemic cardiac output. In this condition, RVEDV is almost the same between 1.5VR and 2VR, and linearly decreases with an increase in the RV stiffness constant in spite of a rapid elevation in RAP. This indicates that RVEDV might be independent of the venous return to RA. Since RAP becomes higher than the atrial pressure of TCPC even in 1.5VR, supraventricular arrhythmias caused by high RAP are liable to occur [2, 5]. In this condition, 1.5VR is considered to have hemodynamics equivalent to APC and needs larger stressed blood volume than does TCPC to maintain systemic arterial pressure (Fig. 3d).

Therefore, TCPC should be chosen for patients with severe RV hypoplasia. In these patients, the arrhythmic events after TCPC are less than that after APC [21, 22]. Although a small pressure gradient between SVC and IVC

remains in 1.5VR, this may not be of clinical significance. Systemic venous collateral channels are expected to be rare, and an increase of RV volume after the operation is unlikely.

Clinical implication

The management strategy for patients with hypoplastic RV has been based on the morphological characteristics, which are dependent on the loading conditions. In contrast, we used a relatively load-independent index, RV stiffness constant, and simulated the postoperative hemodynamics. As a result, we identified the characteristics of hemodynamics after each of the surgical options, and clearly defined the indications of these operations.

Moreover, our results may be useful to theoretically speculate the reason for contrasting clinical findings. Chowdhury and colleagues [2] reported that the event rate of supraventricular arrhythmia was about 15% in the late postoperative phase of 1.5VR. On the other hand, Numata et al. [5] reported higher arrhythmic event rate. In the former report, the patients had a relatively high postoperative RV volume (45–75% of predicted normal RV; Fig. 3c) and a large pressure gradient between SVC and IVC (mean 7.6 mmHg; Fig. 3b) after 1.5VR. Indeed, there was significant pleural effusion in 22.7% of patients. Our results suggest that good systemic cardiac output, low IVC pressure, and high SVC pressure after 1.5VR can be expected under a condition of a relatively small RV stiffness constant. A great difference between SVC and IVC pressures may cause pleural effusion. Therefore, patients in the former report are likely to have low RV stiffness. In the latter report, the average RVEDV at 1 year after 1.5VR was about 50% of normal and there was no obvious collateral after the surgery in the patients examined. These data suggest a high RV stiffness (Fig. 3c), and a small difference between SVC and IVC pressures (Fig. 3b). Since higher arrhythmic event rate is likely to be associated with high RAP in patients with high RV stiffness, we can interpret the marked difference in arrhythmic event rate in these studies based on postoperative hemodynamics. Operations with 1.5 VR in potentially inappropriate patients (i.e., patients with stiffer RV) might impair long-term outcomes by continued high RAP-induced arrhythmia.

If we can assess the RV stiffness constant and other hemodynamic data in a catheter laboratory before operation, we will be able to select the most suitable operation for patients with hypoplastic RV. Recently, noninvasive methods for predicting LV chamber stiffness using echocardiography have been reported [23–25]. For example, LV chamber stiffness has been estimated from the deceleration time of LV early filling, effective mitral area and length. Such a method may be applied to estimate RV chamber stiffness using the deceleration time of RV early filling, effective tricuspid area and length. Moreover, it may be possible to choose an appropriate procedure for individual patients by performing simulation of postoperative hemodynamics from individual data using our model. Further clinical studies are needed to precisely assess the RV stiffness constant, including the above methods.

Limitations

A major limitation of this study is related to the parameters we used for the model. In our model, all parameters other than the RV stiffness constant are fixed. It is reported that RV end-systolic elastance as well as the RV stiffness constant depend upon RV histological changes such as RV hypertrophy [26]. The increase in RV end-systolic elastance moves the beneficial range of 1.5VR toward the stiffer range of the RV stiffness constant. The increase of heart rate also moves the range toward the stiffer range (Table 3). Moreover, ischemia caused by long-standing hypoxemia and hypertension of RV may influence other variables [6]. The existence of pulsatility of the pulmonary circulation may also affect the pulmonary vascular resistance [27]. Tricuspid regurgitation may also impair the postoperative hemodynamics. These limitations may be solved by using the preoperative data of individual patients. Santamore and Burkhoff have already reported the importance of ventricular interdependence using a computer model [13]. However, ventricular interdependence between small hypoplastic RV and relatively large left ventricle may be negligible.

Table 3 The influence of right ventricular end-systolic elastance and heart rate on the beneficial range of the one and a half ventricle repair

	Lower limit of RV stiffness constant (% of normal)	Upper limit of RV stiffness constant (% of normal)
$E_{cs,RV} = 0.7$, HR = 75	150	250
$E_{cs,RV} = 1.4$, HR = 75	200	300
$E_{cs,RV} = 0.7$, HR = 100	175	275

RV Right ventricle, $E_{cs,RV}$ right ventricular end-systolic elastance (mmHg/ml), *HR* heart rate (beats/min)

Conclusion

Using a model analysis, we have shown that the beneficial effect of 1.5VR depends on the RV stiffness constant. 1.5VR is the most beneficial for hypoplastic RV with 150–250% of normal RV stiffness constant. The beneficial range of 1.5VR may also be changed by individual parameters other than the RV stiffness constant, but the beneficial range certainly exists. Therefore, determination of management strategy should be based not only on the morphologic parameters but also on the physiologically determined properties.

Acknowledgments This study was supported by Health and Labor Sciences Research Grants (H18-nano-Ippan-003, H19-nano-Ippan-009, H20-katsudo-Shitei-007 and H21-nano-Ippan-005) from the Ministry of Health, Labor and Welfare of Japan, by Grants-in-Aid for Scientific Research (No. 20390462) from the Ministry of Education, Culture, Sports, Science and Technology in Japan, and by the Industrial Technology Research Grant Program from New Energy and Industrial Technology Development Organization (NEDO) of Japan.

References

1. Yoshimura N, Yamaguchi M, Ohashi H, Oshima Y, Oka S, Yoshida M, Murakami H, Tei T (2003) Pulmonary atresia with intact ventricular septum: strategy based on right ventricular morphology. J Thorac Cardiovasc Surg 126:1417–1426
2. Chowdhury UK, Airan B, Talwar S, Kothari SS, Saxena A, Singh R, Subramaniam GK, Juneja R, Pradeep KK, Sathia S, Venugopal P (2005) One and one-half ventricle repair: results and concerns. Ann Thorac Surg 80:2293–2300
3. Hanley FL (1999) The one and a half ventricle repair-we can do it, but should we do it? J Thorac Cardiovasc Surg 117:659–661
4. Uemura H, Yagihara T, Adachi I, Kagisaki K, Shikata F (2007) Conversion to total cavopulmonary connection after failed one and one-half ventricular repair. Ann Thorac Surg 84:666–668
5. Numata S, Uemura H, Yagihara T, Kagisaki K, Takahashi M, Ohuchi H (2003) Long-term functional results of the one and one half ventricular repair for the spectrum of patients with pulmonary atresia/stenosis with intact ventricular septum. Eur J Cardiothorac Surg 24:516–520
6. Freedom RM (1998) Pulmonary atresia with intact ventricular septum—the significance of the coronary arterial circulation. In: Redington AN, Brawn WJ, Deanfield JE, Anderson RH (eds) The right heart in congenital heart disease. Greenwich Medical Media, London
7. Hanley FL, Sade RM, Blackstone EH, Kirklin JW, Freedom RM, Nanda NC (1993) Outcomes in neonatal pulmonary atresia with intact ventricular septum. A multiinstitutional study. J Thorac Cardiovasc Surg 105:406–427
8. Ashburn DA, Blackstone EH, Wells WJ, Jonas RA, Pigula FA, Manning PB, Lofland GK, Williams WG, McCrindle BW, Congenital Heart Surgeons Study members (2004) Determinants of mortality and type of repair in neonates with pulmonary atresia and intact ventricular septum. J Thorac Cardiovasc Surg 127:1000–1007
9. Burkhoff D, Tyberg JV (1993) Why does pulmonary venous pressure rise after onset of LV dysfunction: a theoretical analysis. Am J Physiol 265:H1819–H1828
10. Morley D, Litwak K, Ferber P, Spence P, Dowling R, Meyns B, Griffith B, Burkhoff D (2007) Hemodynamic effects of partial ventricular support in chronic heart failure: results of simulation validated with in vivo data. J Thorac Cardiovasc Surg 133:21–28
11. Goodwin JA, van Meurs WL, Sá Couto CD, Beneken JE, Graves SA (2004) A model for educational simulation of infant cardiovascular physiology. Anesth Analg 99:1655–1664
12. Migliavacca F, Pennati G, Dubini G, Fumero R, Pietrabissa R, Urcelay G, Bove EL, Hsia TY, de Leval MR (2001) Modeling of the Norwood circulation: effects of shunt size, vascular resistances, and heart rate. Am J Physiol Heart Circ Physiol 280:H2076–H2086
13. Santamore WP, Burkhoff D (1991) Hemodynamic consequences of ventricular interaction as assessed by model analysis. Am J Physiol 260:H146–H157
14. Sagawa K, Maughan L, Suga H, Sunagawa K (1988) Cardiovascular interaction. In: Sagawa K, Maughan L, Suga H, Sunagawa K (eds) Cardiac contraction and the pressure–volume relationship. Oxford University Press, Oxford
15. Walther FJ, Siassi B, King J, Wu PY (1986) Blood flow in the ascending and descending aorta in term newborn infants. Early Hum Dev 13:21–25
16. Wang JJ, Flewitt JA, Shrive NG, Parker KH, Tyberg JV (2006) Systemic venous circulation. Waves propagating on a windkessel: relation of arterial and venous windkessels to systemic vascular resistance. Am J Physiol Heart Circ Physiol 290:H154–H162
17. McElhinney DB, Reddy VM, Hanley FL, Moore P (1997) Systemic venous collateral channels causing desaturation after bidirectional cavopulmonary anastomosis: evaluation and management. J Am Coll Cardiol 30:817–824
18. Gatzoulis MA, Shinebourne EA, Redington AN, Rigby ML, Ho SY, Shore DF (1995) Increasing cyanosis early after cavopulmonary connection caused by abnormal systemic venous channels. Br Heart J 73:182–186
19. Webber SA, Horvath P, LeBlanc JG, Slavik Z, Lamb RK, Monro JL, Reich O, Hruda J, Sandor GG, Keeton BR, Salmon AP (1995) Influence of competitive pulmonary blood flow on the bidirectional superior cavopulmonary shunt. A multi-institutional study. Circulation 92:II279–II286
20. Trusler GA, Williams WG, Cohen AJ, Rabinovitch M, Moes CA, Smallhorn JF, Coles JG, Lightfoot NE, Freedom RM (1990) William Glenn lecture. The cavopulmonary shunt. Evolution of a concept. Circulation 82:IV131–IV138
21. Gelatt M, Hamilton RM, McCrindle BW, Gow RM, Williams WG, Trusler GA, Freedom RM (1994) Risk factors for atrial tachyarrhythmias after the Fontan operation. J Am Coll Cardiol 24:1735–1741
22. Balaji S, Gewillig M, Bull C, de Leval MR, Deanfield JE (1991) Arrhythmias after the Fontan procedure. Comparison of total cavopulmonary connection and atriopulmonary connection. Circulation 84:III162–III167
23. Little WC, Ohno M, Kitzman DW, Thomas JD, Cheng CP (1995) Determination of left ventricular chamber stiffness from the time for deceleration of early left ventricular filling. Circulation 92:1933–1939
24. Lisauskas JB, Singh J, Bowman AW, Kovács SJ (2001) Chamber properties from transmitral flow: prediction of average and passive left ventricular diastolic stiffness. J Appl Physiol 91:154–162
25. Garcia MJ, Firstenberg MS, Greenberg NL, Smedira N, Rodriguez L, Prior D, Thomas JD (2001) Estimation of left ventricular operating stiffness from Doppler early filling deceleration time in humans. Am J Physiol Heart Circ Physiol 280:H554–H561
26. Gaynor SL, Maniar HS, Bloch JB, Steendijk P, Moon MR (2005) Right atrial and ventricular adaptation to chronic right ventricular pressure overload. Circulation 112:I212–I218
27. Szabó G, Buhmann V, Graf A, Melnitschuk S, Bährle S, Vahl CF, Hagl S (2003) Ventricular energetics after the Fontan operation: contractility-afterload mismatch. J Thorac Cardiovasc Surg 125:1061–1069

Structural Heterogeneity in the Ventricular Wall Plays a Significant Role in the Initiation of Stretch-Induced Arrhythmias in Perfused Rabbit Right Ventricular Tissues and Whole Heart Preparations

Kinya Seo, Masashi Inagaki, Satoshi Nishimura, Ichiro Hidaka, Masaru Sugimachi, Toshiaki Hisada, Seiryo Sugiura

Rationale: Mechanical stress is known to alter the electrophysiological properties of the myocardium and may trigger fatal arrhythmias when an abnormal load is applied to the heart.

Objective: We tested the hypothesis that the structural heterogeneity of the ventricular wall modulates globally applied stretches to create heterogeneous strain distributions that lead to the initiation of arrhythmias.

Methods and Results: We applied global stretches to arterially perfused rabbit right ventricular tissue preparations. The distribution of strain (determined by marker tracking) and the transmembrane potential (measured by optical mapping) were simultaneously recorded while accounting for motion artifacts. The 3D structure of the preparations was also examined using a laser displacement meter. To examine whether such observations can be translated to the physiological condition, we performed similar measurements in whole heart preparations while applying volume pulses to the right ventricle. At the tissue level, larger stretches (≥20%) caused synchronous excitation of the entire preparation, whereas medium stretches (10% and 15%) induced focal excitation. We found a significant correlation between the local strain and the local thickness, and the probability for focal excitation was highest for medium stretches. In the whole heart preparations, we observed that such focal excitations developed into reentrant arrhythmias.

Conclusions: Global stretches of intermediate strength, rather than intense stretches, created heterogeneous strain (excitation) distributions in the ventricular wall, which can trigger fatal arrhythmias. (*Circ Res.* 2010;106:176-184.)

Key Words: stretch-induced arrhythmia ■ mechanoelectric feedback ■ optical mapping

Alterations to the mechanical state of the myocardium affect its electrophysiological properties, a phenomenon termed mechanoelectric feedback (MEF).[1,2] MEF is considered to play a significant role in the genesis of cardiac rhythm disturbances in various disease states, such as myocardial infarction and heart failure, in which myocardial tissues are subjected to abnormal loading conditions.[3–5] This speculation is supported by previous observations that in myocardial infarction, ventricular ectopic excitations are initiated by acute stretches of the border zone between the infarct and the normal myocardium.[6–8] A more definite causality is suspected in the etiology of commotio cordis, where sudden death occurs owing to a nonpenetrating chest wall impact in the absence of injury to the ribs, sternum, and heart.[9,10] Using anesthetized juvenile swine, Link et al[10] found that ventricular fibrillation can be produced by a baseball strike, and examined the effects of the phase, strength and speed of the strike for the induction of arrhythmias.

To elucidate the mechanisms underlying MEF and related arrhythmias, extensive studies have been carried out using various preparations from various species, including rabbits, lambs and dogs.[11–13] Stretch-activated channels (SACs) have been regarded as the most likely candidates for the primary transducers of mechanical stress.[14–16] Although such findings at the molecular level can account for changes in the action potential duration, amplitude, effective refractory period and resting potential induced by mechanical interventions at the cellular level, we still face a huge gap between these laboratory findings and clinical arrhythmias observed at the organ level. In this context, Franz et al[17] investigated the effects of increases in ventricular volume and pressure on epicardial monophasic action potentials in both isolated cross-circulated hearts and

Original received January 17, 2008; resubmission received June 26, 2009; revised resubmission received October 23, 2009; accepted October 27, 2009.

From the Department of Human and Engineered Environmental Studies (K.S., T.H., S.S.), Graduate School of Frontier Sciences, The University of Tokyo, Chiba; Department of Cardiovascular Dynamics (K.S., M.I., I.H., M.S.), National Cardiovascular Center Research Institute, Osaka; and Department of Cardiovascular Medicine (S.N.), The University of Tokyo, Japan.

Correspondence to Masashi Inagaki, Department of Cardiovascular Dynamics, National Cardiovascular Center Research Institute, 5-7-1 Fujishirodai, Suita, Osaka 565-8565, Japan; E-mail masashii@ri.ncvc.go.jp or to Seiryo Sugiura, Department of Human and Engineered Environmental Studies, Graduate School of Frontier Sciences, The University of Tokyo 5-1-5 Kashiwanoha, Kashiwa, Chiba 277-8563, Japan; E-mail sugiura@k.u-tokyo.ac.jp

Circulation Research is available at http://circres.ahajournals.org

DOI: 10.1161/CIRCRESAHA.109.203828

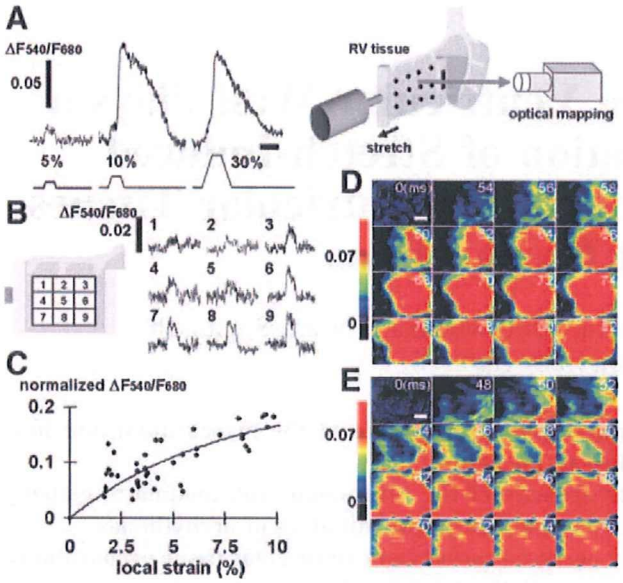

Figure 1. Alterations in the electric response in a cardiac tissue. A, Ratiometric optical signals ($\Delta F_{540}/F_{680}$) in response to 5%, 10%, and 30% stretches from left to right. Scale bar: 100 ms. B, Spatiotemporal pattern of the depolarizations (typical optical signals in each segment) in response to a 5% stretch. C, Relationship between the changes in the normalized optical signals and the local strain under the excitation threshold (n=5). The smooth curve through the data points was fitted with a nonlinear regression model. D and E, Representative action potentials and optical maps in response to 10% and 30% stretches, respectively. The stretch starts at 0 ms. Scale bar: 4 mm.

in situ canine hearts to clearly demonstrate the manifestation of MEF. However, these volume and/or pressure alterations do not allow detailed evaluation of the changes in myocardial stress or strain, which are believed to be the keys for establishing a link between the macroscopic and microscopic phenomena.

To elucidate how the cellular responses to stretches lead to arrhythmias in the heart, we focused on the morphology of tissue preparations and its role in the modulation of the electric responses. We developed an experimental set-up in which controlled uniaxial stretches were applied to crystalline perfused rabbit ventricular walls while monitoring the local strain. The use of optical transmembrane potential mapping combined with a tissue tracking technique enabled us to examine the relationship between local strain and excitation of the myocardium. By applying acute stretches of varying amplitudes, we demonstrate that global stretches applied to the ventricular wall tissue can create strain dispersion in the heterogeneous structure of the ventricular wall and that mechanical insults of intermediate, rather than intense, strength induce focal excitation, thus potentially triggering fatal arrhythmias. Finally, using whole heart preparations, we confirm that only medium stretches of the myocardium can evoke spiral wave formation.

Methods

Japanese white rabbits weighing 2.4 to 2.9 kg were used. The distribution of strain and the transmembrane potential were simultaneously recorded while applying an acute stretch to right ventricle (RV) tissue preparations. The 3D structure of the preparations was also examined. Similar measurements were conducted in whole heart preparations while applying acute volume pulses to the RV.

An expanded Methods section is available in the Online Data Supplement at http://circres.ahajournals.org.

Non-standard Abbreviations and Acronyms

MEF	mechanoelectric feedback
SAC	stretch-activated channel
RV	right ventricle

Results

Effect of the Stretch Amplitude on Excitation of the Tissue

To elucidate the relationship between the electric response and the stretch level, we measured the optical transmembrane potential signals of stretched tissues. Figure 1 shows representative transmembrane potential signals in response to stretches of varying amplitudes. When a uniaxial stretch with a small amplitude (5%) was applied, the myocardial tissue was depolarized but an action potential did not develop (Figure 1A, left). The distribution of these depolarizations was heterogeneous and the amplitudes of these depolarizations had a positive dependence on the local strains (n=5) (Figure 1B and 1C). However, above a certain level of amplitude (≥10%), we observed focal excitation (development of an action potential in less than 4 segments of 9 blocks) (Figure 1A, middle; Figure 1D). A larger stretch (30%) only induced multiple occurrences of excitation in the tissue (Figure 1E). Figure 2A shows the relationship between the probability of tissue excitation (development of an action potential in at least one locus within the tissue) and the amplitude of the stretch applied (global strain). We found a fairly abrupt transition in the tissue responses to a uniaxial stretch (n=7). Specifically, excitation was rare when the amplitude was small (5%), but its rate increased with stretches in the medium range (10% and 15%) to reach 100% (sure observation) in response to large stretches (20%, 25% and 30%).

The use of a trapezoidal command with constant rates of rise and fall necessarily made the entire duration of the stretch longer for larger stretches, which may thus have led to modulation of the responses of the myocardium through different mechanisms. To exclude these possibilities, we applied stretches of varying amplitudes while keeping the entire duration constant at 50 ms. We found similar responses, thereby indicating that the amplitude rather than the duration is the major determinant of stretch-induced activation of the myocardium (Online Figure V, A). We also confirmed that stretches applied during the action potentials could modulate their shapes, and sometimes found stretch-activated depolarizations followed by premature ventricular contractions (Online Figure V, B).

Relationship Between Stretch-Induced Excitation and Epicardial Local Strain

We also evaluated the relevance between stretch-activated excitation and epicardial local strain (n=7). To compare the

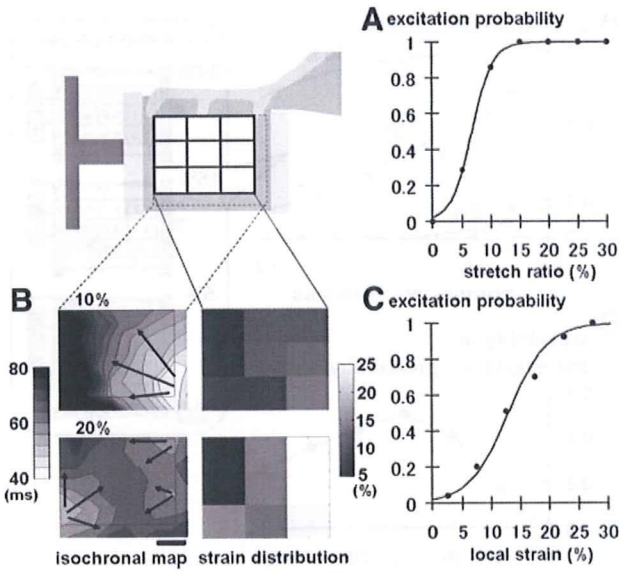

Figure 2. Electric responses and strain distributions. A, Probability that an action potential develops in at least 1 region of the whole tissue as a function of global stretch (n=7). The smooth curve through the data points was fit with a logistic regression model. B, Representative isochronal maps of a transmembrane potential showing the point of initial depolarization (left) and distributions of local strain (right). Top and bottom show 10% and 20% stretch, respectively. Scale bar: 4 mm. C, Relationship between the probability of stretch-induced excitation in the local area and the strain in the corresponding area (n=7). The smooth curve through the data points was fit with a logistic regression model.

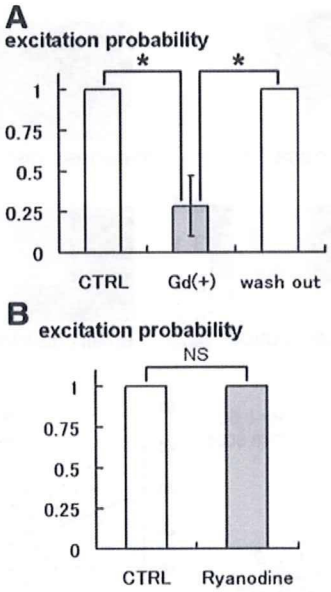

Figure 3. Modulation of stretch-induced excitation by drugs. A, Effect of Gd^{3+} on the probability of stretch-induced excitation after a 15% stretch (n=7). *$P<0.05$. CTRL indicates control condition. B, Effect of ryanodine on the probability of stretch-induced excitation after a 15% stretch (n=3).

strain distribution with the isochronal electric responses, the whole tissue area was divided into 9 blocks and the average strain value in each block was shown in grayscale. The local strain maps at each level of stretch with the corresponding isochronal maps are shown in Figure 2B (right). Initial excitation tended to take place at the locus of high strain (top: right lower block with 14% strain; bottom: left lower block with 14% strain; right upper 2 blocks with 23% and 24% strains). The excitation probability was clearly found to be more prominent for higher strains (Figure 2C), when the probability of local excitation was plotted as a function of the corresponding local strain (n=7).

Involvement of SACs in Stretch-Induced Excitations

To examine the involvement of SACs in the genesis of stretch-induced excitation, we repeated the experiments with a 15% stretch in the presence of 10 μmol/L Gd^{3+}, a blocker of nonspecific SACs. Gd^{3+} inhibited the stretch-induced excitation by 71.4±18.4% compared with the control condition and its effect was reversed by washout of Gd^{3+} (Figure 3A; n=7; $P<0.01$, Gd(+) versus control condition and washout). We also administered ryanodine to examine whether stretch-induced Ca^{2+} release from the sarcoplasmic reticulum and the triggered activity are involved in the activation process. When we applied 15% stretches, action potentials developed similarly in both ryanodine-treated and untreated (control condition) tissues (Figure 3B; n=3).

Strain Distribution and Tissue Structure

Because we applied uniaxial stretches to the ventricular tissue, the strain distribution on the epicardial surface was most probably created by heterogeneity within the tissue structure. To clarify the relationships between the strain distribution and the tissue structure, we measured the thickness distribution in each preparation using a laser displacement meter (Figure 4A; n=7). We divided the tissue into 9 blocks and calculated the average thickness in each block to facilitate comparisons with the strain data. Figure 4B shows a comparison between the thickness and local strain distributions after a 10% stretch from a single experiment. We found that the strain was high in regions where the tissue thickness was thin. For further comparisons between the tissue structure and the strain, we calculated the normalized thickness value of each block (mean thickness value of each block relative to the mean thickness value of all the blocks). Figure 4C summarizes the relationships between the local strain and the local thickness under different levels of stretch. Local strain was negatively correlated with the local thickness, which supported our hypothesis (10% stretch: n=7, $r=-0.52$, $P<0.0001$; 20% stretch: n=7, $r=-0.53$, $P<0.0001$).

Heterogeneous Excitation in Accordance With the Tissue Thickness and Stretch Level

We then plotted the relationship between the local wall thickness and the probability of stretch-induced local excitation for various levels of stretches (Figure 5A; n=7; closed circles, 5% stretch; closed triangles, 15% stretch; open circles, 30% stretch). When the applied stretch was small (5%), there was hardly any excitation (low probabilities over the entire range of thickness) because the local strain was below the threshold. As the amplitude of the stretch increased, the probability of excitation started to rise from the

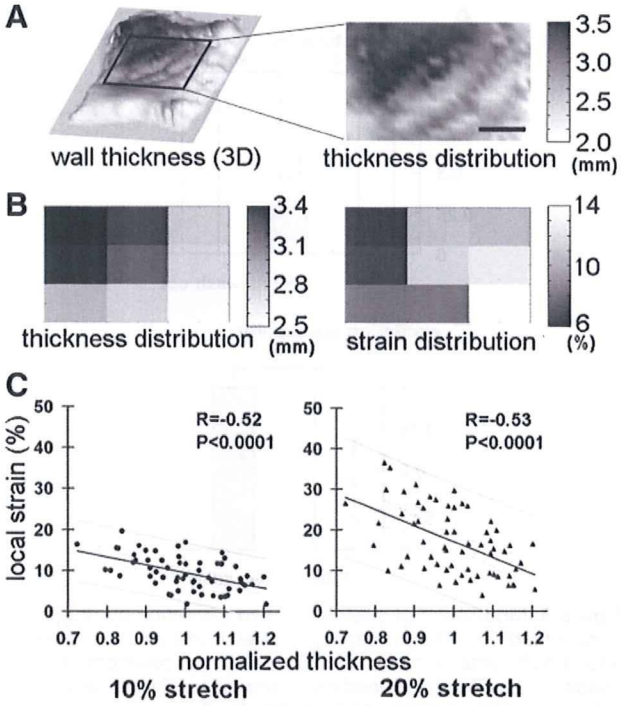

Figure 4. Thickness and local strain distributions of cardiac tissue. A, Representative case of the wall thickness distribution (laser-scanned data). Scale bar: 4 mm. B, Thickness distribution (left) and strain distribution (right) in response to a global 10% stretch in a representative experiment. C, Relationship between the normalized wall thickness and local strain in response to 10% (left) and 20% (right) global stretches. Lines are linear regression lines (10% stretch: n=7, $r=-0.52$, $P<0.0001$; 20% stretch: n=7, $r=-0.53$, $P<0.0001$).

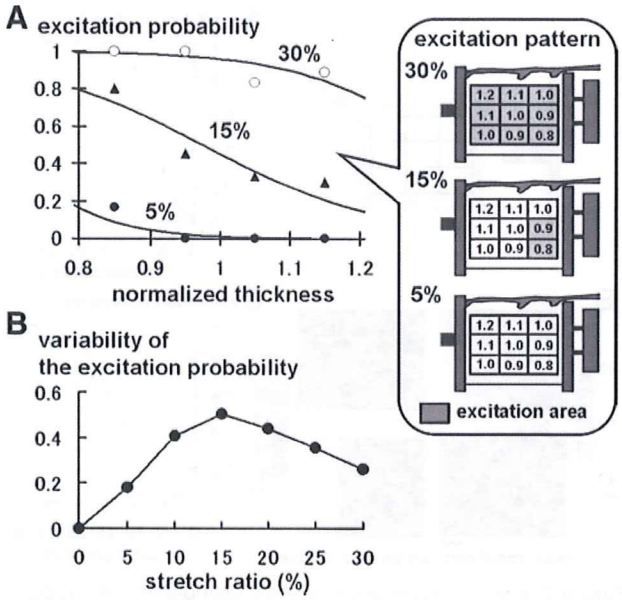

Figure 5. Relationship between the probability of focal excitation and the stretch amplitude. A, Probabilities of stretch-induced local excitation as a function of the relative wall thickness for 5% (closed circles), 15% (closed triangles), and 30% (open circles) stretches (n=7). The smooth curves through the data points were fit with logistic regression models. Right, Distributions of the wall thicknesses, in which the segments where the action potentials developed are depicted in gray for 30% (top), 15% (middle), and 5% (bottom) stretches. B, From the data shown in A, the variability of the probability for the development of local excitation over the entire range of wall thickness was plotted as a function of the global stretch (n=7). Heterogeneous excitation is induced by a stretch of intermediate amplitude rather than a large stretch.

thin area (15%) and all areas were finally excited in response to a large stretch (30%). We calculated the variability (standard deviation) of the excitation probability over the entire thickness range for each stretch amplitude, and these data are plotted in Figure 5B (n=7). In regions of small (5%) or large (30%) stretches, the variability was low (0.18 or 0.26) because the whole tissue was either unresponsive or responsive to the stretch, respectively, whereas heterogeneous excitation was achieved in response to a stretch of intermediate amplitude (0.50 on 15% stretch).

Stretch-Induced Focal Excitations Develop Into Reentrant Arrhythmias in the Ventricle

To examine whether the findings at the tissue level are applicable to more physiological situations, we applied volume pulses to the RV in whole heart preparations and recorded the transmembrane potential responses. Figure 6A and 6B shows representative optical signals in response to 2 different amplitudes of volume pulses. When we applied a small volume pulse (0.5 mL), virtually no response was observed. However, local excitation (excitation from less than one-third of all the blocks) was induced by a 1.0-mL volume pulse (Figure 6A), and a large volume pulse (2.0 mL) elicited excitation from a larger area simultaneously (global excitation) (Figure 6B). The corresponding thickness distribution in the optically mapped region revealed that the focal excitation originated from a thin region (Figure 6C). As summarized in Figure 6D (n=6), focal excitation was only induced with pulses of intermediate volumes (1.0 and 1.5 mL). Structural measurements revealed that such focal excitations tended to take place in regions where the wall thickness was thinner (Figure 6E; n=6, $P<0.05$), similar to the case for the tissue preparations. All of these findings were in accordance with the tissue experiments, thus confirming that only global stretches of medium intensity can induce focal excitation in the ventricular wall.

Focal excitation is a prerequisite for the initiation of reentrant arrhythmias, but may not fulfill the conditions. Therefore, we hypothesized that when the propagation of the focal excitations induced by medium mechanical stimuli interacts with the preceding electric activations, it can develop to fatal reentrant arrhythmias. To assess this hypothesis, we applied the volume pulses to the RV for 50 ms at various coupling intervals (90 to 130 ms) with a preceding electric stimulus. Similar to the electric "pinwheel experiment" protocol,[18] this protocol involves the simultaneous establishment of a spatial gradient of momentary stretch-induced excitability together with a spatial gradient of refractoriness induced by the prior passage of an activation. As shown in Figure 7A, a 1.5-mL volume pulse after a 110-ms coupling interval initiated vortex-like reentrant waves pivoting around phase singularities. As clearly shown in Figure 7B, a large volume pulse (2.0 mL) never elicited arrhythmias, whereas an intermediate volume pulse (1.5 mL) applied after a proper coupling interval (110 ms) triggered reentrant arrhythmias (n=3, 66.7% probability).

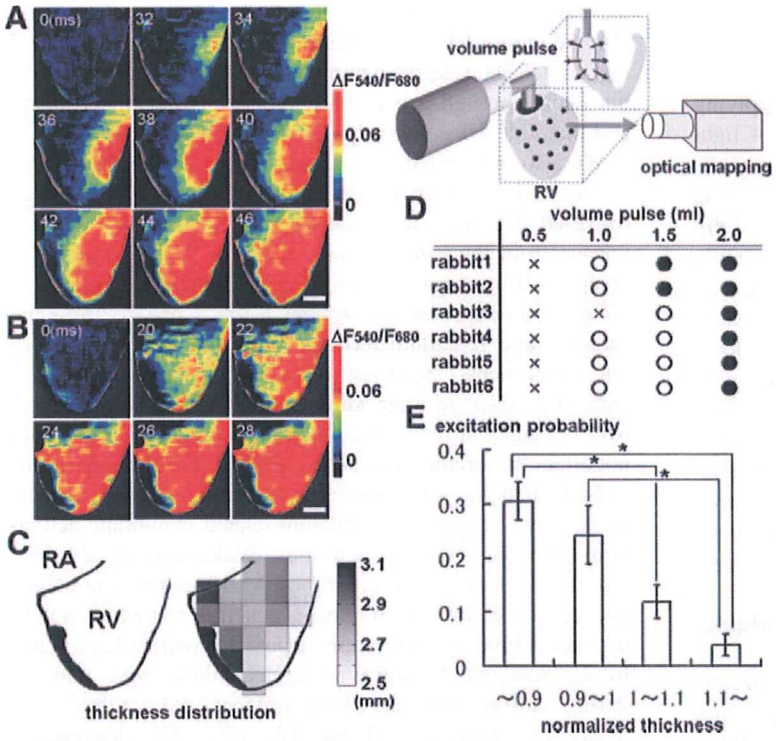

Figure 6. Alterations in the electric responses in a whole heart preparation. A and B, Representative optical maps of the responses of the RV to volume pulses of 1.0 mL (A) and 2.0 mL (B). The stretches start at 0 ms. Scale bar: 4 mm. C, Corresponding thickness distribution in the ventricle. RA indicates right atrium; RV, right ventricle. D, Response patterns to stretches in 6 rabbit hearts. Crosses indicate no excitation; focal excitation, open circles; global excitation, closed circles. E, Excitation probability for each normalized thickness range in the initiation of focal excitation (n=6). *$P<0.05$.

Discussion

In the present study, we simultaneously measured the transmembrane potentials and local strains while applying uniaxial stretches of varying amplitudes to rabbit RV wall tissue to clarify the linkage of electric activity between cells and organs. The use of optical transmembrane potential mapping coupled with local strain measurements based on bead markers enabled us to record the strain–electric response relationship of myocardial tissue. In addition, structural measurements of the preparations suggested that the complex architecture of the ventricular wall could cause heterogeneous strain responses to mechanical stimuli, thereby leading to the initiation of focal excitation. We confirmed this hypothesis under more physiological conditions by successfully inducing reentrant arrhythmias using a volume pulse of medium amplitude.

Optical Mapping of the Transmembrane Potential

Owing to its high temporal and spatial resolutions, optical recording of transmembrane potentials has been widely used, but most studies have only dealt with immobile preparations where the motion was inhibited mechanically and/or pharmacologically.[19–21] These stabilizations of the preparations were conducted to prevent motion artifacts caused by changes in the fluorescence intensity along the light path, and also

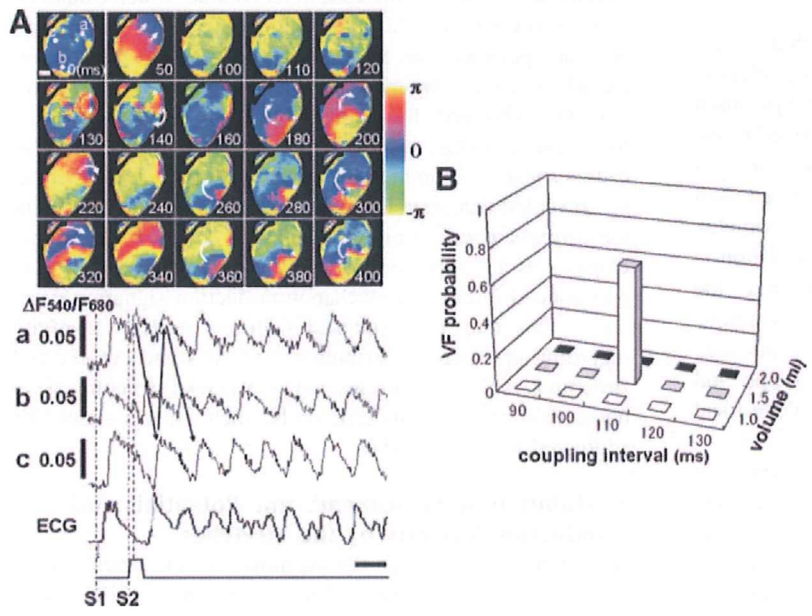

Figure 7. Initiation of spiral waves by volume pulses. A, Representative phase maps of spiral wave formation. The volume pulse was applied at 110 ms after the electric stimulus. Scale bar: 4 mm. a through c represent the ratiometric optical signals ($\Delta F_{540}/F_{680}$) for the corresponding positions shown in the 0-ms optical map (top left). The electric stimulus starts at 0 ms. The ECG is shown at the bottom. Scale bar: 100 ms. *Phase singularity points. B, Excitation probabilities in relation to the coupling intervals and the intensities of the volume pulses (n=3).

changes in the *x-y* position. In the present study, we tried to account for the motion-induced contamination of optical signals by using 2 methods to accurately evaluate the transmembrane potentials of the local myocardium while applying a stretch to the whole tissue. First, the fluctuation of light intensity was cancelled by ratiometry of the 2 emission bands of the fluorescent indicators. Second, by using the affine transformation based on motion tracking, we successfully traced the tissue points, presumably a cluster of specific myocytes, during a stretch and induced contraction, and showed the sequential changes in the transmembrane potential in the reference position. As shown in Figure 1A, the local action potential triggered by the stretch reconstructed with these techniques is similar to that recorded by an electrode with its clear zero phase characteristics. Compared with a previous study of the local response of electric activity to a linear acute stretch using a pair of electrodes in isolated frog ventricular tissue at only 2 points,[22] detailed maps of the action potentials were obtained with the present technique.

Heterogeneity in the Tissue Structure for Bridging Cellular Responses to Arrhythmias

Although the activity of ion channels was not directly measured, the present results were consistent with previous studies demonstrating the involvement of SACs in MEF. Zeng et al[23] recorded the stretch-dependent inward current, which was blocked by Gd^{3+} in rat cardiac myocytes. They also observed that a 10% stretch induced an immediate contraction of the myocytes. Although the threshold for excitation varies among studies, similar observations were made for rat (>20%),[24] guinea pig (20% to 25%),[25] and frog (15%)[26] myocytes. In our probability curves of stretch-induced excitation for both whole tissues and segments (Figure 2A and 2C), the transition from nonresponse to excitation took place within a similar range of stretch amplitudes. Furthermore, the response was inhibited by Gd^{3+} and recovered by washout of the agent. Taken together, these results suggest that a uniaxial stretch applied to the tissue induces strain in the myocytes, which in turn triggers the activation of molecular mechanotransducers, most probably SACs.

The use of a tissue preparation provided us with a unique opportunity to elucidate the relationships among electric excitation, global strain and local strain on the epicardial surface. Although a uniaxial global stretch was applied to the preparation, excitation was usually only induced in a limited area where the local strain was high. We speculate that such heterogeneity in the strain distribution reflects the complex structure of the ventricular wall, such that the excitation is initiated in regions where the wall is thin. Whereas the complex structure of the ventricles normally allows vigorous contraction, different hemodynamic overloads in diseased states lead to abnormalities in the ventricular shape and regional wall motion,[27,28] which may sometimes evoke focal excitations.

We must consider the possibility that the presence of damaged ends may have caused an abnormal strain near the tissue supports to initiate the excitation from the edge region. However, the locus of focal excitation always followed the thickness distribution, such that the excitation was elicited in the center of a preparation that had a thin central region (Online Figure VI, A). Furthermore, ter Keurs et al[29] reported that stretch-induced excitations from the damaged myocardium occur through a calcium-related triggering mechanism, and that Gd^{3+} does not suppress these phenomena.

We also considered the relevance of a Ca^{2+}-related mechanism to our experiments. Fujiwara et al[30] showed that triggered activities were subsequently evoked by a Ca^{2+} release from the sarcoplasmic reticulum through ryanodine receptors. Furthermore, some previous studies reported that an acute stretch can also trigger a Ca^{2+} release from the sarcoplasmic reticulum through ryanodine receptors.[31,32] In our experiments, however, the stretch-induced excitations were still observed after administration of ryanodine. Moreover, changes in the extracellular calcium concentration did not affect the stretch-induced excitability. These observations indicate that the stretch-induced excitations in our experiments were not linked to calcium-related membrane activations like the triggered activities. Wakayama et al[33] also reported that excitation caused by MEFs can be the consequence of a quick stretch release, which is related to stretch-dependent binding and release of Ca^{2+} to contractile proteins. In our experiments, however, the excitations were initiated during the rise or plateau of the stretches, and not during the release of the stretches (Figure 1A, right). This discrepancy may be caused by the fact that the excitation as a consequence of a quick release in the previous report was only observed at a high Ca^{2+} concentration (5.2 ± 0.73 mmol/L), whereas our experiments were carried out with a lower Ca^{2+} concentration (1.8 mmol/L). These observations indicate that the stretch-induced excitations observed in our study are not related to the release of Ca^{2+} to contractile proteins following the stretch release.

Translation of data obtained with tissue preparations to the intact heart requires consideration in terms of both the magnitude and the nature of the deformation. A volume pulse of 2.0 mL induced global excitation, the effect caused by a 20% stretch of the tissue. However, if we simply assume a spherical ventricle, a 20% increase in its circumference would lead to an almost 70% increase in its volume, which cannot be accounted for by the 2.0-mL volume pulse in the rabbit RV. We can speculate that the thinner RV free wall was preferentially stretched whereas the thick ventricular septum remained unchanged. In addition to the stretch applied to the tissue preparations, volume expansion of the ventricle also causes shear and compression of the wall. In fact, Isenberg et al[34] revealed that stretch and compression activated different ion currents in guinea pig ventricular myocytes. Furthermore, Gopalan et al[35] reported that transverse stretches have more pronounced effects on mechanotransduction signaling pathways. This may be associated with the stretch sensitivity regarding the spatial distributions of SACs and cytoskeletal structures. Although currents and cytoskeletal structures were not examined in the present study, such aspects should be addressed in future studies.

Modulation of Transmembrane Potentials and Conduction Velocity by the Stretches

Although we focused on the magnitude of the stretch in the present study, care was taken to eliminate confounding

factors. Fasciano and Tung[22] revealed that the stretch speed significantly affects the stretch-induced excitability. In this context, we made the speed of the stretch constant in all the experiments (Online Figure IV). We checked the influence of the stretch duration in another set of experiments in which the stretch duration was made constant at 50 ms. We confirmed that these 2 types of protocols did not cause any significant differences in the excitability induced by the stretch.

We also examined the effect of the stretch timing relative to the action potentials. Similar to previous reports,[17,36] stretches applied in each phase (2, 3 and 4) of the action potentials modulated the transmembrane potentials differently (Online Figure V, B).

We calculated the conduction velocity of the focal excitations elicited by 10% stretches and compared it with that elicited by an electric stimulus (Online Figure VI, B). In these experiments, the spread of conduction between 2 recording positions (crosses) was completed during the stretch plateau. Although the number of observations was limited owing to the technical difficulty, we confirmed that the conduction velocities of the stretch-induced excitations in both the horizontal and vertical directions tended to be slower (31.7% and 38.7% decrease in vertical and horizontal direction, respectively). In addition, we also examined the relationship between the normalized dV/dt_{max} (evaluated by the time derivative of the ratiometric optical signal, dF/dt_{max}) of action potential upstrokes and local strains. Normalized dV/dt_{max} of the action potential upstroke was decreased in regions where local strain was high (Online Figure VII). Although the effects of stretches on the conduction velocity are still controversial,[37] conduction slowing has been reported in previous studies.[21,38] Eijsbouts et al[38] reported that the anisotropic nature in the heterogeneous wall thickening may play an important role in conduction disturbances attributable to dilation. Geometric and structural changes during an acute stretch should be some of the causes of this effect, and SACs and the intracellular calcium dynamics may also be involved in this phenomenon. In either case, such changes in the propagation characteristics could also contribute to the development of reentrant arrhythmias.

Clinical Implications

When a mechanical stimulus of moderate amplitude was applied to the ventricular wall, local excitation was induced in regions where the wall thickness was thin and, if other facilitatory conditions were met, it was propagated to the adjacent area to develop into fatal arrhythmias. We expect that further increases in the intensity of the stimulus would induce multiple excitations to exaggerate the electric heterogeneity, thereby increasing the possibility of arrhythmias. However, if a very intense stimulus is applied, the whole tissue can be synchronously excited, which considerably decreases the possibility of arrhythmias (Figure 5B). Interestingly, we can see a similar tendency in the relationship between the ventricular fibrillation probability and the rise in ventricular pressure produced by a baseball impact in an experimental study on commotio cordis by Link et al,[10] who did not provide any mechanistic comments.

In this study, a volume pulse of 1.5 mL at a 110-ms coupling interval after the last electric stimulus initiated a reentrant arrhythmia. No reentrant arrhythmia, however, was induced by 1.0-mL volume pulses that triggered focal excitations when applied at 500-ms coupling intervals. These findings probably arise from a dependence of the strength of the mechanical stimuli required to generate focal activity on the phase of the action potential at which it is applied. In contrast to the protocol (a), in which the pulses were applied to the fully relaxed ventricle after a long coupling interval (500 ms), we confirmed that the myocardium in activated states has higher thresholds for activation (Online Figure VIII). Based on these observations, a 1.0-mL volume pulse cannot initiate the excitation with coupling intervals from 90 to 130 ms, whereas a 1.5-mL volume pulse can initiate focal excitations with coupling intervals of >100 ms. Although the focal excitations were frequently initiated with coupling intervals of >120 ms, the excitations did not develop into reentrant arrhythmias because a unidirectional conduction block cannot be formed at these timings. Owing to the trapezoidal volume change and viscoelastic nature of the tissue, the effect of the volume pulse was realized with some delay. In fact, although we applied a volume pulse after a 110-ms coupling interval, excitation was initiated at around 130 ms corresponding to the late phase 2 of the action potential. We speculate that these findings correspond to the observation that ventricular fibrillations were triggered when the chest wall impacts were applied during the vulnerable portion of the T wave.[9]

Our present results suggest that the complex structure of the ventricular wall functions to modulate a mechanical impact and create a heterogeneous excitation distribution in response to a stimulus of intermediate intensity, rather than an intense stimulus, to initiate ventricular fibrillation in otherwise healthy young subjects.

The structural complexity of the ventricular wall may also contribute to the genesis of arrhythmias in old myocardial infarctions. Regarding myocardial infarction, it is considered that the conduction abnormality in the infarct area acts as the substrate for arrhythmias,[39] but its trigger still remains unclear. Bogen et al[40] reported that a large mechanical load is added to the border zone in regions where the wall thickness is thin in systole. Moreover, Josephson[41] revealed that arrhythmias are often initiated from these borders. Calkins et al[8] observed that ventricular dilation shortens the refractoriness of the surviving myocardium in the infarct area rather than the healthy myocardium. Taken together, the following scenario is conceivable. In an old myocardial infarction, a systolic rise in ventricular pressure can induce a large stretch in the functional border zone, where the wall thickness is thin to provoke an ectopic excitation, which may develop into fatal reentrant arrhythmias promoted by the conduction abnormality in the infarct area.

In either case, the structural and/or functional heterogeneity of the myocardial tissue serves to create a heterogeneous strain distribution, and establishes a MEF-mediated electrophysiological dispersion in the tissue, which is known to be a potent substrate for arrhythmias.

Study Limitations

Although the use of flattened tissue preparations made it easy to evaluate local strain, the results cannot be translated directly to the clinical setting where volume/pressure loading or external compression distorts the ventricular tissue in a complex manner. Furthermore, although uniaxial stretches may cause 3D strain within the tissue with reductions in the width and thickness, these effects were not taken into consideration. On the other hand, the intact heart preparations pose a problem for potential mapping and the measurement of strain. In either case, because the action potentials and strains were recorded at the epicardial surface, we did not evaluate the heterogeneity in the transmural structure from the epicardium to the endocardium. Furthermore, as stated above, we did not measure the ion currents in response to the stretches, although they seemed to greatly promote our understanding of stretch-induced arrhythmias in the intact heart. Finally, we only used the RV in our experiments based on our assumption that the RV is more vulnerable to mechanical stimuli because of its weak elasticity, and stretch-induced arrhythmias could also be evoked in the left ventricle.

In summary, a global stretch applied to the ventricular wall tissue can create a heterogeneous strain distribution in the heterogeneous structure of the ventricular wall. Such heterogeneity in the strain distribution can lead to local excitation, which in turn leads to fatal reentrant arrhythmias.

Sources of Funding

This work was supported in part by a Japan Heart Foundation Young Investigator's Research Grant (to K.S.), Research Fellowships from the Japan Society for the Promotion of Science (JSPS) for Young Scientists (to K.S.), JSPS KAKENHI (21590920) (to M.I.), a Health and Labour Sciences Research Grant for Research on Medical Devices for Improving Impaired QOL (to M.I., M.S., and T.H.), grants from the Core Research for Evolutional Science and Technology of the Japan Science and Technology Agency (to T.H.), and JSPS KAKENHI (B) (20300152) (to S.S.).

Disclosures

None.

References

1. Taggart P, Lab M. Cardiac mechano-electric feedback and electrical restitution in humans. *Prog Biophys Mol Biol.* 2008;97:452–460.
2. Ravens U. Mechano-electric feedback and arrhythmias. *Prog Biophys Mol Biol.* 2003;82:255–266.
3. Tomaselli GF, Marban E. Electrophysiological remodeling in hypertrophy and heart failure. *Cardiovasc Res.* 1999;42:270–283.
4. Janse MJ. Electrophysiological changes in heart failure and their relationship to arrhythmogenesis. *Cardiovasc Res.* 2004;61:208–217.
5. Aimond F, Alvarez JL, Rauzier JM, Lorente P, Vassort G. Ionic basis of ventricular arrhythmias in remodeled rat heart during long-term myocardial infarction. *Cardiovasc Res.* 1999;42:402–415.
6. Coronel R, Wilms-Schopman FJ, deGroot JR. Origin of ischemia-induced phase 1b ventricular arrhythmias in pig hearts. *J Am Coll Cardiol.* 2002;39:166–176.
7. Dillon SM, Allessie MA, Ursell PC, Wit AL. Influences of anisotropic tissue structure on reentrant circuits in the epicardial border zone of subacute canine infarcts. *Circ Res.* 1988;63:182–206.
8. Calkins H, Maughan WL, Weisman HF, Sugiura S, Sagawa K, Levine JH. Effect of acute volume load on refractoriness and arrhythmia development in isolated, chronically infarcted canine hearts. *Circulation.* 1989; 79:687–697.
9. Link MS, Wang PJ, Pandian NG, Bharati S, Udelson JE, Lee MY, Vecchiotti MA, VanderBrink BA, Mirra G, Maron BJ, Estes NA III. An experimental model of sudden death due to low-energy chest-wall impact (commotio cordis). *N Engl J Med.* 1998;338:1805–1811.
10. Link MS, Maron BJ, Wang PJ, VanderBrink BA, Zhu W, Estes NA III. Upper and lower limits of vulnerability to sudden arrhythmic death with chest-wall impact (commotio cordis). *J Am Coll Cardiol.* 2003;41: 99–104.
11. Chen RL, Penny DJ, Greve G, Lab MJ. Stretch-induced regional mechanoelectric dispersion and arrhythmia in the right ventricle of anesthetized lambs. *Am J Physiol Heart Circ Physiol.* 2004;286:H1008–H1014.
12. Hansen DE, Craig CS, Hondeghem LM. Stretch-induced arrhythmias in the isolated canine ventricle. Evidence for the importance of mechanoelectrical feedback. *Circulation.* 1990;81:1094–1105.
13. Parker KK, Taylor LK, Atkinson JB, Hansen DE, Wikswo JP. The effects of tubulin-binding agents on stretch-induced ventricular arrhythmias. *Eur J Pharmacol.* 2001;417:131–140.
14. Sachs F. Stretch-activated channels in the heart. In: Kohl P, Sachs F, Franz MR, eds. *Cardiac Mechano-Electric Feedback and Arrhythmias: From Pipette to Patient.* Philadelphia, Pa: Elsevier Sauders; 2005;2–10.
15. Ward ML, Williams IA, Chu Y, Cooper PJ, Ju YK, Allen DG. Stretch-activated channels in the heart: contributions to length-dependence and to cardiomyopathy. *Prog Biophys Mol Biol.* 2008;97:232–249.
16. Kohl P, Day K, Noble D. Cellular mechanisms of cardiac mechanoelectric feedback in a mathematical model. *Can J Cardiol.* 1998;14: 111–119.
17. Franz MR, Burkhoff D, Yue DT, Sagawa K. Mechanically induced action potential changes and arrhythmia in isolated and in situ canine hearts. *Cardiovasc Res.* 1989;23:213–223.
18. Winfree AT. Electrical instability in cardiac muscle: phase singularities and rotors. *J Theor Biol.* 1989;138:353–405.
19. Kanai A, Salama G. Optical mapping reveals that repolarization spreads anisotropically and is guided by fiber orientation in guinea pig hearts. *Circ Res.* 1995;77:784–802.
20. Moreno J, Zaitsev AV, Warren M, Berenfeld O, Kalifa J, Lucca E, Mironov S, Guha P, Jalife J. Effect of remodelling, stretch and ischaemia on ventricular fibrillation frequency and dynamics in a heart failure model. *Cardiovasc Res.* 2005;65:158–166.
21. Sung D, Mills RW, Schettler J, Narayan SM, Omens JH, McCulloch AD. Ventricular filling slows epicardial conduction and increases action potential duration in an optical mapping study of the isolated rabbit heart. *J Cardiovasc Electrophysiol.* 2003;14:739–749.
22. Fasciano RW II, Tung L. Factors governing mechanical stimulation in frog hearts. *Am J Physiol.* 1999;277:H2311–H2320.
23. Zeng T, Bett GC, Sachs F. Stretch-activated whole cell currents in adult rat cardiac myocytes. *Am J Physiol Heart Circ Physiol.* 2000;278: H548–H557.
24. Nishimura S, Kawai Y, Nakajima T, Hosoya Y, Fujita H, Katoh M, Yamashita H, Nagai R, Sugiura S. Membrane potential of rat ventricular myocytes responds to axial stretch in phase, amplitude and speed-dependent manners. *Cardiovasc Res.* 2006;72:403–411.
25. Kamkin A, Kiseleva I, Isenberg G. Stretch-activated currents in ventricular myocytes: amplitude and arrhythmogenic effects increase with hypertrophy. *Cardiovasc Res.* 2000;48:409–420.
26. Tung L, Sliz N, Mulligan MR. Influence of electrical axis of stimulation on excitation of cardiac muscle cells. *Circ Res.* 1991;69:722–730.
27. Katz AM, Katz PB. Homogeneity out of heterogeneity. *Circulation.* 1989;79:712–717.
28. Remme EW, Nasb MP, Hunter PJ. Distributions of myocytes stretch, stress, and work in models Of normal and infarcted ventricles. In: Kohl P, Sachs F, Franz MR, eds. *Cardiac Mechano-Electric Feedback and Arrhythmias: From Pipette to Patient.* Philadelphia, Pa: Elsevier Sauders; 2005;381–391.
29. ter Keurs HE, Zhang YM, Miura M. Damage-induced arrhythmias: reversal of excitation-contraction coupling. *Cardiovasc Res.* 1998;40: 444–455.
30. Fujiwara K, Tanaka H, Mani H, Nakagami T, Takamatsu T. Burst emergence of intracellular Ca2+ waves evokes arrhythmogenic oscillatory depolarization via the Na+-Ca2+ exchanger: simultaneous confocal recording of membrane potential and intracellular Ca2+ in the heart. *Circ Res.* 2008;103:509–518.
31. Iribe G, Ward CW, Camelliti P, Bollensdorff C, Mason F, Burton RA, Garny A, Morphew MK, Hoenger A, Lederer WJ, Kohl P. Axial stretch of rat single ventricular cardiomyocytes causes an acute and transient increase in Ca2+ spark rate. *Circ Res.* 2009;104:787–795.

32. Tatsukawa Y, Kiyosue T, Arita M. Mechanical stretch increases intracellular calcium concentration in cultured ventricular cells from neonatal rats. *Heart Vessels*. 1997;12:128–135.
33. Wakayama Y, Miura M, Sugai Y, Kagaya Y, Watanabe J, ter Keurs HE, Shirato K. Stretch and quick release of rat cardiac trabeculae accelerates Ca2+ waves and triggered propagated contractions. *Am J Physiol Heart Circ Physiol*. 2001;281:H2133–H2142.
34. Isenberg G, Kazanski V, Kondratev D, Gallitelli MF, Kiseleva I, Kamkin A. Differential effects of stretch and compression on membrane currents and [Na+]c in ventricular myocytes. *Prog Biophys Mol Biol*. 2003;82:43–56.
35. Gopalan SM, Flaim C, Bhatia SN, Hoshijima M, Knoell R, Chien KR, Omens JH, McCulloch AD. Anisotropic stretch-induced hypertrophy in neonatal ventricular myocytes micropatterned on deformable elastomers. *Biotechnol Bioeng*. 2003;81:578–587.
36. Zabel M, Koller BS, Sachs F, Franz MR. Stretch-induced voltage changes in the isolated beating heart: importance of the timing of stretch and implications for stretch-activated ion channels. *Cardiovasc Res*. 1996;32:120–130.
37. Mills RW, Narayan SM, McCulloch AD. The effects of wall stretch on ventricular conduction and refractoriness in the whole heart. In: Kohl P, Sachs F, Franz MR, eds. *Cardiac Mechano-Electric Feedback and Arrhythmias: From Pipette to Patient*. Philadelphia, Pa: Elsevier Sauders; 2005;127–136.
38. Eijsbouts SC, Majidi M, van Zandvoort M, Allessie MA. Effects of acute atrial dilation on heterogeneity in conduction in the isolated rabbit heart. *J Cardiovasc Electrophysiol*. 2003;14:269–278.
39. Aizawa M, Aizawa Y, Chinushi M, Takahashi K, Shibata A. Conductive property of the zone of slow conduction of reentrant ventricular tachycardia and its relation to pacing induced terminability. *Pacing Clin Electrophysiol*. 1994;17:46–55.
40. Bogen DK, Rabinowitz SA, Needleman A, McMahon TA, Abelmann WH. An analysis of the mechanical disadvantage of myocardial infarction in the canine left ventricle. *Circ Res*. 1980;47:728–741.
41. Josephson ME, Harken AH, Horowitz LN. Endocardial excision: a new surgical technique for the treatment of recurrent ventricular tachycardia. *Circulation*. 1979;60:1430–1439.

SUPPLEMENT MATERIAL

Detailed Methods

Tissue preparation

Japanese white rabbits weighing 2.4–2.9 kg were anesthetized with intravenous sodium pentobarbital (50 mg/kg). After a thoracotomy was performed, the heart was quickly excised, and the aorta was connected to a Langendorff apparatus and perfused at a pressure of 66 mmHg with Tyrode's solution (pH 7.40) containing (mmol/L): 130 NaCl, 4 KCl, 1 $MgCl_2$, 1.2 NaH_2PO_4, 1.8 $CaCl_2$, 5.6 glucose and 24 $NaHCO_3$. The perfusion solution was equilibrated with 95% O_2/5% CO_2 at 37°C.

After the heart was allowed to recover in fresh Tyrode's solution for 10 min, the right ventricular (RV) free wall was peeled off from the heart taking care to avoid damage to the coronary artery. We trimmed the RV free wall to a rectangular shape while the connection to the left ventricle (LV) remained intact (Online Figure IA). The tissue was glued to tissue supports, as shown in Online Figure IA, with a cyanoacrylate tissue adhesive (Vetbond™; 3M, St. Paul, MN). The left edge of the tissue was attached to a linear motor (ET-126A; Labworks Inc., Costa Mesa, CA) for application of linear stretches to the tissue and a displacement transducer (IW12; TWK-Elektronik, Düsseldorf, Germany) was used to measure the length of the various stretches. We set the right coronary artery in parallel with the stretch direction. The reaction force in the direction of the stretch was also measured with a force transducer (FORT-1000; World Precision Instruments, Sarasota, FL). To make the tissue taut, we applied a force of 10 gf, which defined our 0% stretch level. Zirconia beads (diameter, 0.5 mm) were attached to the myocardial surface as landmarks for motion tracking and strain measurement. At this point, the curvature of the RV surface was negligible and we assumed that the preparation was flat. To avoid tissue damage from the direct electrical stimuli, two Ag-AgCl electrodes were attached to the LV wall for ventricular pacing. The shapes of the action potentials measured on the RV surface under these conditions did not differ appreciably from those in whole heart preparations, thereby indicating that the procedures for the RV free wall preparation did not cause significant damage to the tissue and that the electrical activation was propagated from the LV normally (Online Figure II). ECG was recorded by electrodes. The measured signals were digitized at 2 kHz with a 12-bit analog-to-digital converter and stored in the hard disk of a personal computer (PC).

All experimental procedures were performed in strict accordance with the Guiding Principles for the Care and Use of Animals in the Field of Physiological Sciences approved by the Physiological Society of Japan and were approved by the National Cardiovascular Center Research Institutional Committee.

Whole heart preparation

Whole hearts from Japanese white rabbits weighing 2.4–2.9 kg were connected to a Langendorff apparatus using the same method described above. After the heart was stabilized in fresh Tyrode's solution for 10 min, a compliant polyvinyl chloride balloon was inserted into the RV. The balloon was connected to a water-filled piston pump system based on an electromagnetic shaker and a linear power amplifier (ARB-126; AR Brown, Tokyo, Japan) for rapid volume changes (Online Figure III). The volume changes were controlled by monitoring the motion of the piston with a displacement transducer (IW12; TWK-Elektronik). Volume commands were generated by a computer. Zirconia beads (diameter, 0.5 mm) were attached to the myocardial surface as landmarks. In these experiments, however, they were only used for correction of motion artifacts because the curvature of the RV surface prevented their use for strain measurement. Two Ag-AgCl electrodes were attached to the LV apex for ventricular pacing. ECG was recorded by electrodes. The measured signals were digitized at 2 kHz with a 12-bit analog-to-digital converter and stored in the hard disk of a PC.

Optical mapping of transmembrane potentials on the epicardial surface

Schematic representations of the experimental systems used are shown in Online Figure IB and Online Figure III. The methods used for recording transmembrane activity from the arterially perfused RV free walls and whole hearts were similar to those described in a previous study [1]. The tissues or hearts were loaded with a voltage-sensitive dye, di-4-ANEPPS (5 μmol/L), for 20 min. The epicardial surfaces of the tissues or hearts were illuminated by filtered excitation light (480±10 nm) obtained from bluish-green light-emitting diodes (Nichia Chemical Industries, Tokushima, Japan). The emitted fluorescent light was collected by a high numerical aperture complex photographic lens (50mm F/1.2; Nikon, Tokyo, Japan) and was split by a dichroic mirror (580nm; Andover, Salem, NH) and narrowed down to two frequency bands (540±20 nm and 680±20 nm; Andover, Salem, NH) through bandpass filters. The dual-wavelength lights were simultaneously collected by two independent complementary metal oxide semiconductor (CMOS) cameras with image intensifiers (FASTCAM-Ultima; Photron, Tokyo, Japan). The optical images were captured at a speed of 500 frames/s and a resolution of 256×256 pixels and stored in a PC. No electromechanical uncoupling agents were used.

Image processing

To account for motion artifacts caused by the stretch or contraction from the optical signals, we used ratiometry combined with a recently developed motion tracking technique [1]. For motion tracking, the initial images were chosen as a reference. In these reference images, several bead landmarks were selected manually. The corresponding positions of landmarks in the current image were automatically determined by finding the optimal local correlation of the surrounding image. We used template matching of the image of each bead with its surroundings between the resting state and the stretched state to determine the displacement of the landmark beads at high resolution (0.12 mm). These positional data were used for two purposes. First, the distances between the markers in the stretched

state were divided by the corresponding distances in the reference state to yield the epicardial local strain. Second, we used the positional data to determine the affine transformation matrices for the geometric distortion during the stretch or contraction. By using affine transformation, we mapped the sequential changes in fluorescence in the original resting geometry. Subsequently, ratiometry with numerator wavelengths of 540±20 nm and denominator wavelengths of 680±20 nm was used to remove the artifacts caused by motion along the light path. After the spatial and temporal filtering, we constructed isochronal maps of activation to determine the excitation points or the excitation propagation pattern. Moreover, phase analysis was used to study the initiation of excitations and the pattern of wave propagations [2].

Stretch protocol for tissue preparations

The protocol for applying stretch to tissue preparations is shown in Online Figure IVA. In each experiment, a stretch pulse (S2) was preceded by at least 20 electrical pulses (S1: amplitude, 2 mA; duration, 2 ms; 2 Hz) to stabilize the tissue conditions. We applied a trapezoidal command signal with a fixed plateau phase (P) at 50 ms and a rise and fall rate of 0.5% of the tissue length/ms. The amplitude was set at 5%, 10%, 15%, 20%, 25% or 30% of the tissue length and the sequence was randomized. The coupling interval (I2) between the last S1 and S2 was set at 500 ms.

Volume pulse protocol for whole heart preparations

Two types of protocols were used for whole heart preparations (Online Figure IVB). In protocol (a), after hearts were paced electrically from the RV apex 20 times, volume pulses of varying amplitudes (0.5, 1.0, 1.5 and 2.0 ml) were applied in the diastolic phase (500 ms after the electrical stimulus) to observe the stretch-induced depolarization. Because the rise and fall rate of the pulses was made constant at 0.1 ml/ms and the total duration of the pulse was also made constant (60 ms), the plateau phase (P) varied from 20~50 ms. In protocol (b), after 20 electrical stimuli from the RV apex, volume pulses of varying amplitudes (1.0, 1.5 and 2.0 ml) and constant duration (50 ms) were applied at various coupling intervals (90~130 ms). The rise and fall rate of the pulses was made constant at 0.2 ml/ms.

Pharmacological intervention

To elucidate whether the stretch-induced excitation originated from SACs, we examined the effects of Gd^{3+}. To avoid precipitation of $GdCl_3$, an oxygenated physiological salt solution (pH 7.40) was used containing (mmol/L): 137 NaCl, 5.4 KCl, 1.8 $CaCl_2$, 0.5 $MgCl_2$, 5 Hepes and 5.6 glucose. This solution was bubbled with 100% O_2 at 37°C [3, 4]. After perfusion with the salt solution in the presence of 10 μmol/L Gd^{3+} for 10 min, we recorded the optical signals in response to a 15% stretch of the ventricular tissue. We then repeated the same procedure after 15 min of perfusion with the salt solution without Gd^{3+} (washout).

We further examined the effects of ryanodine, a blocker of Ca^{2+} release channels on the sarcoplasmic

reticulum. Briefly, we applied a 15% stretch to the tissue in the presence of 200 μmol/L ryanodine.

3D structure recording system

After the measurements of both tissues and whole heart preparations, the RV wall was isolated from the heart and glued to the bottom of a saline-filled chamber via its epicardial surface with the Vetbond™ cyanoacrylate tissue adhesive. Care was taken to protect the tissue against drying by sealing the chamber with a thin polyvinylidene chloride film during the measurements. The chamber was placed on an automatic X-Y stage (KST-50XY; Sigma Koki, Tokyo, Japan) and the endocardial surface was scanned with a laser displacement meter (LK-G30; Keyence, Osaka, Japan) every 0.5 mm in both the X and Y directions to construct a wall thickness map. We discarded the thickness data for the margin because deformation caused by trimming and gluing was observed in this area.

Data analysis

To examine the inter-relationships among the isochronal map of electrical excitation, the strain distribution and the thickness distribution, each specimen was divided into 3×3 blocks of equal size and the spatially averaged data in each block were used for analyses.

To compare the optical membrane potentials among the preparations, we used the normalized value defined as follows:

$$\text{Normalized } \Delta F_{540}/F_{680} = \frac{\text{Mean } \Delta F_{540}/F_{680} \text{ of depolarization}}{\text{Peak } \Delta F_{540}/F_{680} \text{ of action potential}}$$

where $\Delta F_{540}/F_{680}$ is the ratiometric value of the optical signal. To normalize $\Delta F_{540}/F_{680}$, we used the amplitude of preceding action potential initiated by the electrical stimulus (S1).

To compare the thickness distributions among the preparations, we used the normalized thickness value of each block defined as follows:

$$\text{Normalized thickness value} = \frac{\text{Mean thickness value of each block (mm)}}{\text{Mean thickness value of all the blocks (mm)}}.$$

To compare dF/dt max (time derivative of the ratiometric optical signal) among the preparations, we used normalized values defined as follows:

$$\text{Normalized dF/dt max} = \frac{\text{Max } d(F_{540}/F_{680})/dt \text{ of action potential upstroke}}{\text{Peak } \Delta F_{540}/F_{680} \text{ of action potential}}.$$

To estimate the probability of tissue excitation (y) as a function of the stretch ratio, strain or normalized thickness (x), the following logistic regression curve with a two-parameter equation was used:

$$y = \frac{1}{1+\exp(a+bx)}$$

where a and b are regression coefficients.

To evaluate the relationship between changes in the membrane potentials (y) (under threshold) and local strain (x), we used the following non-linear regression curve with a two-parameter equation: